Hindawi
Shock and Vibration
Volume 2021, Article ID 1945385, 12 pages
https://doi.org/10.1155/2021/1945385

Research Article

Push Plate Test of CRTS II Slab Ballastless Track: Theoretical Analysis, Experiments, and Numerical Simulation

Yu Liu,[1,2] **Qianqi Xu**,[1] **Xiaodan Sun**,[1] **Guotao Yang**,[3] **and Guotang Zhao**[3]

[1]*School of Civil Engineering, Southwest Jiaotong University, Chengdu 610031, China*
[2]*Key Laboratory of High-Speed Railway Engineering, Ministry of Education, Southwest Jiaotong University, Chengdu 610031, China*
[3]*Department of Science, Technology and Information Technology, China Railway, Beijing 100844, China*

Correspondence should be addressed to Yu Liu; liuyu@swjtu.edu.cn

Received 28 April 2021; Accepted 7 June 2021; Published 21 June 2021

Academic Editor: Honglue Qu

Push plate test is a powerful tool to evaluate the interfacial bond performance of China railway track structure type-II slab ballastless track structure (CRTS II SBTS). However, there is still a lack of theoretical explanation of the push plate test. In this paper, a linear proportional distribution method is proposed in terms of a series of analytical formulas to describe the interfacial force-displacement variation of CRTS II SBTS in different damage stages of the horizontal push plate test. The force-displacement relationship established by the linear proportional distribution method agrees well with that observed in full-scale test. The horizontal push plate test is then simulated, in which a bilinear cohesive zone model (CZM) was adopted to simulate the interface within track structure. The parameters of the CZM are calculated based on the force-displacement curves obtained from scale push plate test. Particularly, the normal cohesive parameters are determined based on the scale vertical push plate test instead of the traditional splitting tensile test. The simulation proves that both the maximum affected length in the undamage stage and the maximum damaged length in the damage stage depend rather on the interfacial stiffness and the material parameters of SBTS than the horizontal load. These two lengths given by the simulation are close to those defined by the proposed linear proportional distribution method. This indicates the reliability of the proposed method and the capability of scale push plate test in determining cohesive parameters.

1. Introduction

China railway track structure type-II slab ballastless track structure (CRTS II SBTS) is widely used for high-speed railway (HSR) of China because it can provide high rail smoothness and ensure high comfort, stability, and safety of high-speed train. It is firstly applied in the Beijing-Tianjin HSR in 2008 and then utilized in the Beijing-Shanghai HSR in 2011. The total mileage of the CRTS II SBTS application is over 9,000 km, about 26% of the total mileage of China HSR. CRTS II SBTS is a layered structure that consists of the track slab made of reinforced, the cement asphalt mortar (referred to as CA mortar hereinafter) layer, and the base made of concrete, as illustrated in Figure 1. A perfect bond of the interfaces between the CA mortar layer and the track slab as well as the base is the key to ensure the stability and durability of CRTS II SBTS. However, under the daily cyclic thermal load [1, 2] and the repeated living load of the train [3], the interfacial bond is likely to degrade or fail, leading to the discontinuous and nonuniform distribution of the interfacial stress, and hence the initiation or expansion of delamination [4].

In the early stage of the CRTS II SBTS application, the interfacial bond behavior was evaluated by a single index of interfacial bond strength observed in in-situ push plate test [5]. The bond behavior between the track slab and the CA mortar layer was considered qualified if the interfacial bond strength meets the standard. However, the single index of interfacial bond strength is incapable to explain a large number of interfacial damage and delamination that are

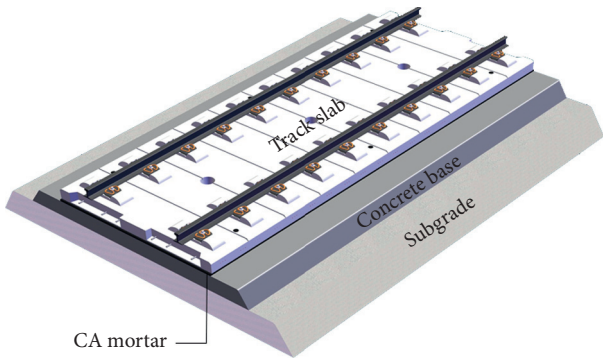

Figure 1: Diagram of the CRTS II SBTS on subgrade.

observed in CRTS II SBTS in recent years. Therefore, finite element analysis (FEA) together with fracture mechanics theory has been introduced to interpret the initiation and evolution of the interfacial damage [6, 7]. In the FEA, CRTS II SBTS is regarded as a layered composite structure. The interface between the CA mortar layer and the track slab is simulated by the cohesive zone model (CZM) [8, 9]. The parameters of the CZM are usually determined by the push plate test of CRTS II SBTS. However, because of the high cost and the high requirements for the test site and test equipment, only very rare push plate test are full scale that use real CRTS II SBTS [10, 11]. Most existed experimental studies are scale push plate test [12] which are relatively cheaper, simpler, and practical to be repeated in large quantities. One problem of the scale push plate test is that if the specimen is too small, the interfacial bond may fail too quick after loading to obtain the expected force-displacement relationship curve. Compared to the numerous experimental studies of push plate test, there is no study that presents a theoretical explanation for the interfacial force-displacement variation during push plate test. Considering the cost of the experiment, it is worth trying to establish theoretical formulas to describe the interfacial force-displacement relationship of CRTS II SBTS. In addition, a theoretical solution of the interfacial force-displacement relationship would help to validate whether the commonly used CZM and the cohesive parameters obtained from push plate test are reliable for the use of FEA.

On the other hand, the push plate test carried out so far are all horizontal push plate test that can only provide tangential force-displacement relationship and tangential cohesive parameters. No vertical push plate test has been reported. The normal cohesive parameters used in most simulations are obtained from splitting tensile test [13–16]. In the splitting tensile test, the normal cohesive parameters are determined based on the normal strain at several specific points. The normal cohesive parameter determined in this way has large randomness because it strongly depends on the bond behavior of the CA mortar of the selected local area. It cannot represent the overall bond behavior of the entire interface and the real changing of the force-displacement variation. To make the FEA of the interfacial damage evolution closer to reality, a real normal force-displacement relationship is required to calculate realistic normal cohesive parameters, which strongly suggests the need to carry out vertical push plate test.

In this paper, the theoretical analysis of the force-displacement variation of the interface during the horizontal push plate test of CRTS II SBTS is conducted. A scale vertical push plate test and a scale horizontal push plate test are carried out to determine the normal and tangential cohesive parameters, respectively. The calculated cohesive parameters are then adopted in the FEA for a CRTS II SBTS model by which the evolution of the interfacial damage is reproduced. The scope of this work is to explore the force-displacement variation during the push plate test, determine the parameters that better describe the interfacial bond behaviour of CRTS II SBTS than the single index of interfacial bond strength, and clarify whether the interfacial parameters obtained from the scale push plate test can be used in the FEA of the full-scale push plate test.

2. Theoretical Analysis of Horizontal Push Plate Test

In this section, the CZM used to describe the bond performance of the interface is introduced and a new method in terms of a series of analytical formulas to construct the force-displacement relationship in the push plate test is proposed.

2.1. Bilinear CZM. The bilinear CZM in fracture mechanics theory is employed to characterize the force-displacement variation in the entire loading process, as shown in Figure 2. Assume that σ_n, σ_t, and σ_s are the interfacial stresses in the normal and two tangential directions, respectively. For a tangentially isotropic interface, $\sigma_t = \sigma_s$. As seen from Figure 2, the force-displacement curve increases linearly at the early stage of loading, with the slope of the stiffness E_n and E_s for the normal and tangential direction, respectively. When the force-displacement curve reaches the peak, the interfacial damage initiates, which can be quantitatively judged by the Quads criterion:

$$\left(\frac{\langle \sigma_n \rangle}{\sigma_n^0}\right)^2 + \left(\frac{\sigma_t}{\sigma_t^0}\right)^2 + \left(\frac{\sigma_s}{\sigma_s^0}\right)^2 \geq 1, \tag{1}$$

where $\langle \sigma_n \rangle = (\sigma_n + |\sigma_n|)/2$. The stress for the moment of the damage initiation is called interfacial strength, σ_n^0 and σ_t^0 for the normal and tangential direction, respectively, while the corresponding displacement is δ_n^0 and δ_s^0, respectively. Therefore, $E_n = \sigma_n^0/\delta_n^0$ and $E_s = \sigma_s^0/\delta_s^0$.

The bilinear CZM also assumes a linear softening evolution after damage initiation. Thus, the stress after damage initiation can be given by

$$\begin{cases} \sigma_n = (1 - D)E_n\delta_n, \\ \sigma_s = (1 - D)E_s\delta_s, \end{cases} \tag{2}$$

where D represents the overall damage in one cohesive element, which is zero initially and then gradually evolves from 0 to 1 upon further loading [17]:

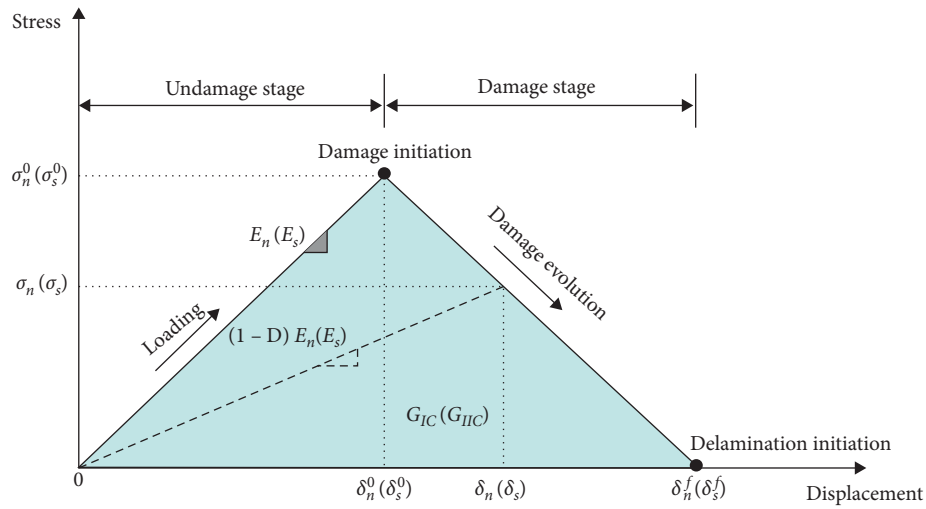

Figure 2: Bilinear CZM for the damage evolution.

$$D = \frac{\delta_m^f\left(\delta_m - \delta_m^0\right)}{\delta_m\left(\delta_m^f - \delta_m^0\right)}, \tag{3}$$

where $m = n$ for the normal direction and $m = s$ for the tangential direction. When D equals to 1, delamination occurs. Assuming δ_n^f and δ_s^f are the normal and tangential displacement for the moment of the delamination occurrence, respectively the fracture toughness in the normal and tangential direction, G_{IC} and G_{IIC}, can be measured by the area of the triangle in Figure 2, $G_{IC} = (1/2)\sigma_n^0\delta_n^f$ or $G_{IIC} = (1/2)\sigma_s^0\delta_s^f$.

2.2. Force-Displacement Variation in Push Plate Test. In this section, the force-displacement relationship of CRTS II SBTS during the horizontal push plate test is theoretically analyzed with the aid of the bilinear CZM. A standard single CRTS II SBTS is 6.45 meter long. For this length, the longitudinal compression deformation of the track slab cannot be neglected in the horizontal displacement of the track slab. The zone with longitudinal compression deformation becomes larger as the loading continues. To sufficiently represent the zone that is affected by the load, a scenario long track slab is assumed. Note that, this long track slab is not actually a longitudinally continuous system of several single track slabs. It is uniform and isotropic without any discontinuity. The stress and displacement of the scenario track slab under horizontal plad is first calculated. Then, the stress and displacement of a single track slab for different damage stages can be determined by directly taking the part on the scenario track slab that is undamaged, partially damaged, or completely damaged. The details of this method, the linear proportional distribution method, are demonstrated below.

In the horizontal push plate test, the force is applied at the leftmost end of the scenario track slab. When the horizontal push force is low and the maximum tangential stress on the track slab is less than σ_s^0, the scenario track slab will not be damaged. The tangential stress distribution along the scenario track slab is as shown in Figure 3(a), with the maximum tangential stress appears at the loading end. Both the displacement and the tangential stress vary linearly on the slab. Assuming the length of the slab that is affected by the horizontal load (with nonzero tangential stress, referred to as the maximum affected length hereinafter) to be L_0 and the right end of L_0 to be the origin of coordinates (point O in Figure 3(a)), the cross-section compressive strain for point x will be

$$\varepsilon_x = \frac{\sigma_x}{E} = \frac{1}{2}\frac{\sigma_s}{E}\frac{x^2}{L_0 h} = \frac{1}{2}\frac{E_s}{E}\frac{x^2}{L_0 h}\delta_s, \tag{4}$$

where h and E are the thickness and elastic modulus of the slab, respectively. Therefore, the longitudinal displacement at the left end of the slab can be calculated by

$$\int_0^{L_0} \varepsilon_x \mathrm{d}x = \int_0^{L_0} \frac{1}{2}\frac{E_s}{E}\frac{x^2}{L_0 h}\delta_s \mathrm{d}x = \frac{1}{6}\frac{E_s}{E}\frac{L_0^3}{L_0 h}\delta_s. \tag{5}$$

At the left end of the slab, equation (5) should be equal to δ_s, which gives

$$L_0 = \sqrt{\frac{6Eh}{E_s}}. \tag{6}$$

As seen from equation (6), L_0 relates only to E, h, and E_s and is not horizontal load dependent.

Once the maximum tangential stress exceeds σ_s^0, damage is initiated at the loading end and the stress at the loading end starts to decrease. As the loading continues, the damage extends towards the other end of the slab and the location of the maximum stress moves towards the other end. At the moment, when the tangential stress at the loading end reduces to zero and the displacement at the loading end equals to δ_s^f, delamination occurs. At this moment, the damage extends to a certain point where the tangential stress equals σ_s^0 and the displacement equals δ_s^0. Taking this point as the origin of coordinates (point O in Figure 3(b)), the left of point O is the maximum damaged zone within which the

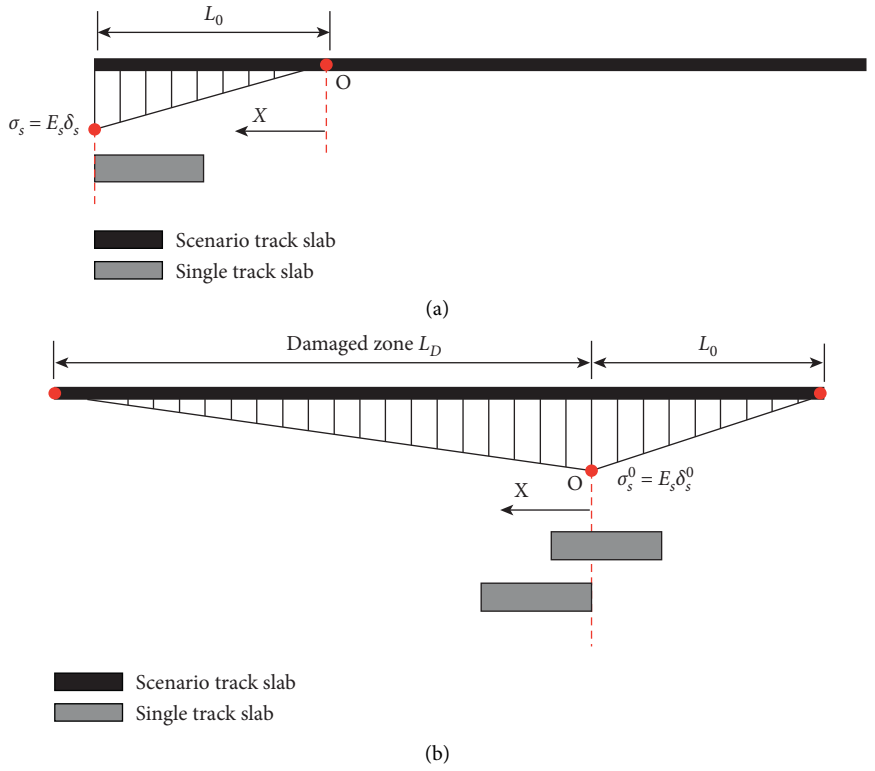

Figure 3: Linear proportional distribution of stress of a single track slab.

stress linearly decreases to zero at the loading end. The right part of point O is not damaged, within which the stress also linearly decreases to zero. The maximum damaged length is assumed to be L_D.

According to the bilinear CZM in Figure 2, the tangential stress in the damage stage is $\sigma_s = \sigma_s^0 \cdot (\delta_s^f - \delta_s)/(\delta_s^f - \delta_s^0)$. At the loading end, $\delta_s = \delta_s^f$; thus, $\sigma_s = 0$. For any x between the loading end and point O, the tangential stress is

$$\sigma_{s\_x} = \left(1 - \frac{x}{L_D}\right)\sigma_s^0. \tag{7}$$

Taking the right portion of point O as the analytical object, the cross-section compressive stress at point O is

$$\sigma_{c\_O} = \frac{\sigma_s^0 L_0}{2h}. \tag{8}$$

Taking the left portion of point O as the analytical object, the cross-section compressive stress at x is

$$\sigma_{c\_x} = \sigma_{c\_O} + \frac{\sigma_{s\_x} + \sigma_s^0}{2} \cdot x. \tag{9}$$

Hence, the compressive deformation at the loading end can be calculated by

$$\int_0^{L_D} \frac{\sigma_{c\_x}}{E} dx = \frac{1}{E}\int_0^{L_D} \left\{\sigma_{c\_O} + \frac{\sigma_{s\_x} + \sigma_s^0}{2} \cdot x\right\} dx = \frac{\sigma_s^0}{2Eh}\left(L_0 \cdot L_D + \frac{2}{3}L_D^2\right). \tag{10}$$

The longitudinal displacement at the loading end equals the sum of the longitudinal displacement at point O and the compressive deformation at the loading end:

$$\delta_s^f = \delta_s^0 + \frac{\sigma_s^0}{2Eh}\left(L_0 \cdot L_D + \frac{2}{3}L_D^2\right). \tag{11}$$

Equation (11) gives

$$\frac{2}{3}L_D^2 + L_0 \cdot L_D = \left(\delta_s^f - \delta_s^0\right)\frac{2Eh}{\sigma_s^0}. \tag{12}$$

Assuming that $\lambda = L_D/L_0$, equation (12) can be further simplified as

$$\frac{2}{3}\lambda^2 + \lambda = \frac{1}{L_0^2}\left(\delta_s^f - \delta_s^0\right)\frac{2Eh}{\sigma_s^0}. \tag{13}$$

According to equation (6), L_0 is fixed for constant E, E_s, and h; thus, equation (13) turns to be

$$\frac{2}{3}\lambda^2 + \lambda - \frac{1}{3}\frac{\delta_s^f - \delta_s^0}{\delta_s^0} = 0, \tag{14}$$

which gives

$$\lambda = \frac{1}{4}\left[-3 + \sqrt{9 + \frac{8\left(\delta_s^f - \delta_s^0\right)}{\delta_s^0}}\right]. \quad (15)$$

As seen from equation (15), L_D is also horizontal load independent. It only depends on E, h, E_s, δ_s^0, and δ_s^f.

Using equations (6) and (15), L_0, L_D, and the displacement and tangential stress at any point on the scenario slab can be determined. On the basis of this, the displacement and stress of a single track slab for different damage stages can be calculated by locating the single track slab on the scenario track slab according to the condition of whether the single track slab is undamaged, partially damaged, or completely damaged.

A single track slab that is not damaged can be considered as being located entirely in the undamaged zone of the scenario track slab, as illustrated in Figure 3(a). The tangential stresses at the left and right end of the single track slab σ_{sl} and σ_{sr} are

$$\begin{aligned} \sigma_{sl} &= E_s\delta_s, \\ \sigma_{sr} &= \frac{L_0 - L}{L_0}E_s\delta_s, \end{aligned} \quad (16)$$

where L is the length of the single track slab. The horizontal load is then calculated by

$$F_H = \frac{2L_0 - L}{2L_0}E_s\delta_s \cdot LB. \quad (17)$$

A single track slab that is damaged can be considered as being located partially or fully in the damaged zone of the scenario track slab, as illustrated in Figure 3(b). For a partially damaged single track slab, σ_{sl} and σ_{sr} are

$$\begin{aligned} \sigma_{sl} &= \frac{L_D - x}{L_D}E_s\delta_s^0, \\ \sigma_{sr} &= \frac{L_0 - (L - x)}{L_0}E_s\delta_s^0, \end{aligned} \quad (18)$$

where x is the length of the portion on the single track slab that is damaged, $x = ((\delta_s - \delta_s^0)/(\delta_s^f - \delta_s^0))L_D$; then, the horizontal load is given by

$$F_H = E_s\delta_s^0 \cdot \left[L - \frac{x^2}{2L_D} - \frac{(L - x)^2}{2L_0}\right]B. \quad (19)$$

If the single track slab is completely damaged, it can be considered as being located entirely in the damaged zone of the scenario slab. Then, σ_{sl} and σ_{sr} are

$$\begin{aligned} \sigma_{sl} &= (1 - D)E_s\delta_s, \\ \sigma_{sr} &= \frac{L_D}{L_D - L}(1 - D)E_s\delta_s, \end{aligned} \quad (20)$$

and the horizontal load will be

$$F_H = \frac{2L_D - L}{2(L_D - L)}(1 - D)E_s\delta_s \cdot LB. \quad (21)$$

The flowchart of the use of the linear proportional distribution method is illustrated in Figure 4. For any single track slab with given E, E_s, and h and cohesive parameters of δ_s^0 and δ_s^f, L_0 and L_D can be determined; hence, the force-displacement relationship can be constructed using equations (17), (19), and (21). The force-displacement curve constructed by this method is compared to that observed in the full-scale push plate test. Two full-scale test are used for the comparison. One is carried out by the Max Bögl company and the other is presented in [10]. The comparison of the force-displacement curves is shown in Figure 5. In general, the theoretical curve constructed by the linear proportional distribution method agrees well with the tested curve. Differences could be observed for the displacement less than 0.5 mm in Figure 5(a). This is not surprising considering the linear assumption of the stress variation in the undamage stage of the bilinear CZM. Differences are also seen between the displacement range of (0.02 mm, 0.32 mm) in Figure 5(b). This may indicate that when the interfacial stiffness (the slope of the curve in the undamage stage) is large, a greater horizontal load than the theoretical estimation is needed to make the damage initiate. Note that, both of the two tested curves exhibit three stages that differ from the two-stage assumption in the bilinear CZM. There is an apparent stage between the undamage stage and damage stage, in which the track slab is partially damaged due to the existence of the longitudinal compression deformation, as revealed in [10]. This stage is well defined by equation (19), which makes the proposed analytical formulas an effective and reliable tool for the quantitative analysis of the entire evolution process of the interfacial damage in the horizontal push plate test.

3. Scale Push Plate Tests for CZM Parameters

The horizontal push plate test is then simulated using the finite element analysis (FEA). In the FEA, the interface between the track slab and the CA mortar layer is simulated using cohesive elements. To determine the cohesive parameters of the CZM, two-scale push plate test are carried out, including a scale vertical push plate test and a scale horizontal push plate test for the determination of the normal and tangential cohesive parameters, respectively. Figure 6(a) shows the scheme and in-situ setup of the scale vertical push plate test. The test is carried out 28 days after the CA mortar is grouted into the track structure. The track slab is lifted vertically with the load applied at the midpoint of the track slab. Two dial gauges are placed 20 cm away from the midpoint at each side. The thicknesses of the track slab and the CA mortar layer are 20 cm and 3 cm, respectively, which are the same as the real track structure. The base is integrally poured with a thickness of 30 cm. In order to meet the requirements of the minimum loading area of the jack in the vertical push plate test and ensure the uniform distribution of the load, a 20 cm by 20 cm loading area is reserved in the middle of the specimen. At each side of the loading

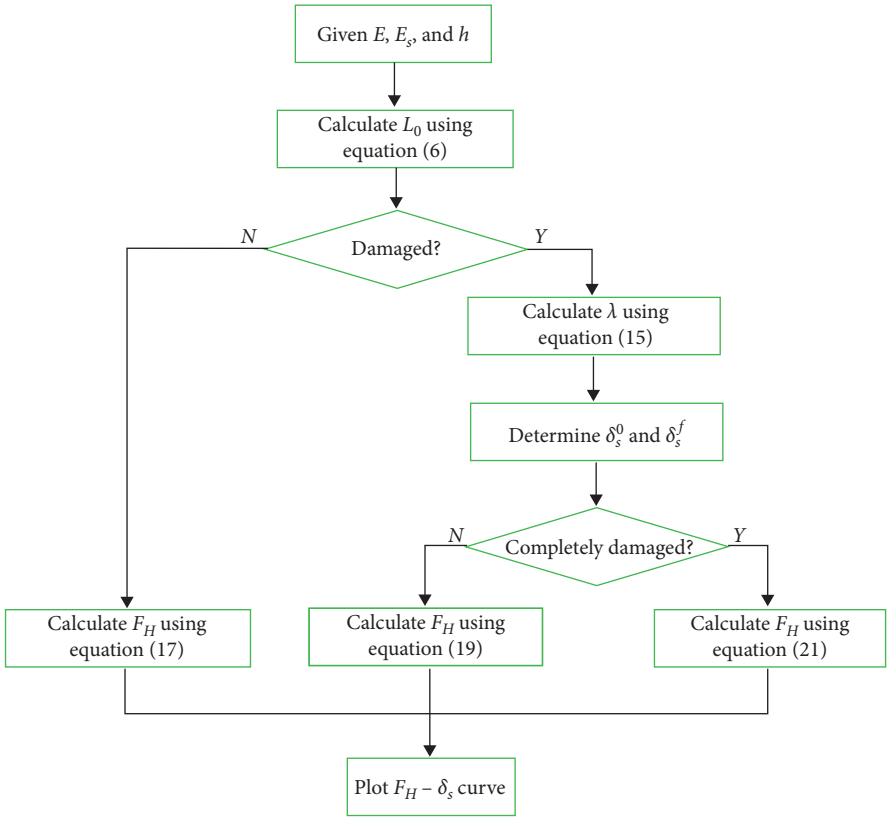

Figure 4: Flowchart of the use of the linear proportional distribution method.

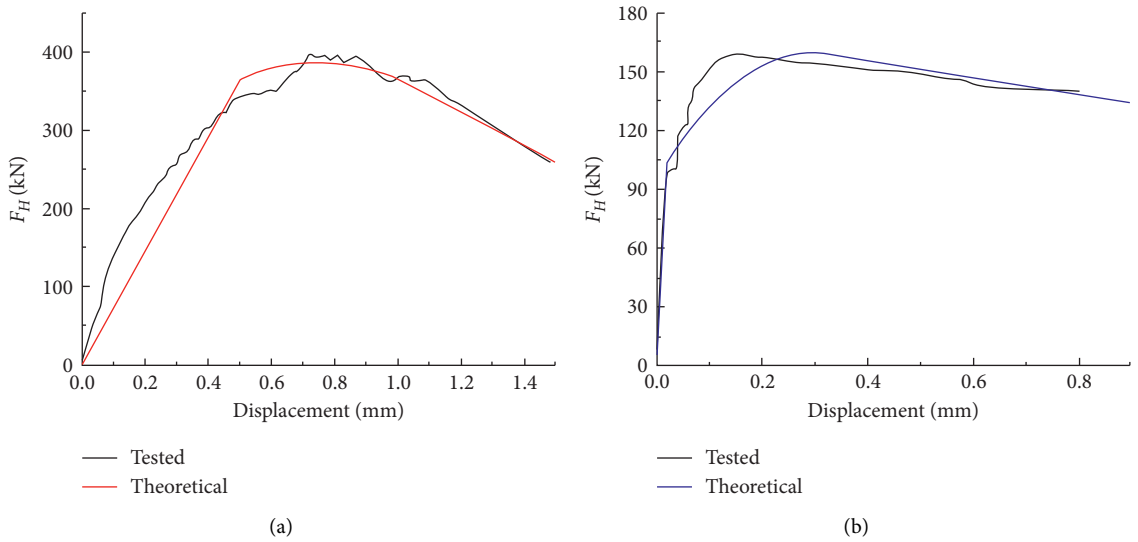

Figure 5: Comparison of force-displacement relationships constructed by the proposed method and full-scale test. (a) Max Bögl company; (b) [10].

area, an area of 20 cm by 20 cm is designed for the track slab to be bonded with the base so that the stress of the interface is uniform and symmetrical. Therefore, the total length of the track slab is 60 cm and the width is 20 cm. Figure 6(b) shows the scheme and in-situ setup of the scale horizontal push plate test. The size of the specimen is the same as that used in the vertical push plate test. The load is horizontally applied at the center of the cross section at one end, and two dial gauges are arranged horizontally at both two ends of the specimen. The relative displacement between the track slab

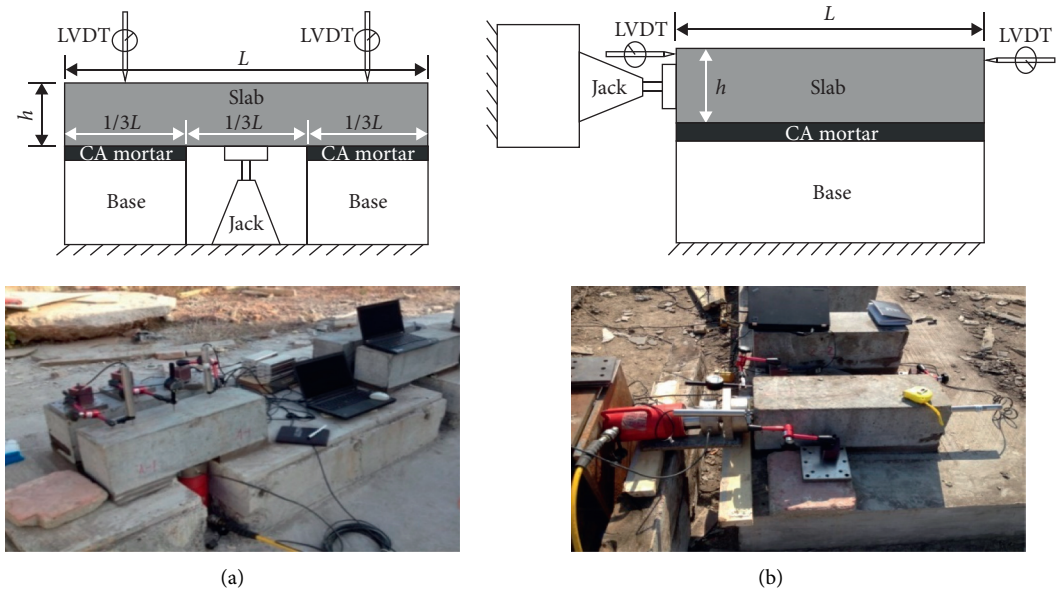

(a) (b)

Figure 6: Scheme and setup of the scale push plate tests. (a) Scale vertical push plate test. (b) Scale horizontal push plate test.

and the base was tested using LVDTs. The jack works synchronously by an automation control system to provide a constant-rate increased load.

Figure 7 shows the force-displacement curve obtained in the scale tests. σ_n^0 and σ_s^0 can be determined by the peak stress of the vertical and horizontal force-displacement curve, respectively. δ_n^0 and δ_s^0 are then identified corresponding to σ_n^0 and σ_s^0, respectively. Afterwards, E_n and E_s can be calculated using $E_n = \sigma_n^0/\delta_n^0$ and $E_s = \sigma_s^0/\delta_s^0$. δ_n^f and δ_s^f are visually picked as the displacement after which there is slight fluctuation in the force-displacement curve. Based on δ_n^f and δ_s^f, G_{IC} and G_{IIC} can be calculated using $G_{IC} = (1/2)\sigma_n^0\delta_n^f$ or $G_{IIC} = (1/2)\sigma_s^0\delta_s^f$. The determined cohesive parameters are also indicated in Figure 7.

4. Simulation of Horizontal Push Plate Test

In this section, the entire evolution of the interfacial damage during the horizontal push plate test is simulated using FEA. The finite element model of CRTS II SBTS, as shown in Figure 8, consists of a 6.45-meter-long track slab, a base of the same length, and a CA mortar layer between the track slab and the base. The track slab, CA mortar layer, and base are established using solid elements. The interface between the track slab and the CA mortar layer is simulated using 1-mm-thick cohesive elements with the parameters illustrated in Figure 7. The elastic modulus for the track slab, CA mortar layer, and base is 3.60×10^4 MPa, 1×10^4 MPa, and 2.20×10^4 MPa, respectively. The corresponding density is 2500 kg/m^3, 1950 kg/m^3, and 2400 kg/m^3, respectively. The initial state of the interface is assumed to be perfectly bonded (no damage), and the nodes at the bottom of the base are fully constrained. In the FEA, the load is applied by gradually increasing the displacement from 0 to 1 mm with an interval of 0.005 mm at one end of the track slab.

Figure 9 shows the simulated interfacial tangential stress σ_s and total stiffness damage D along the track slab for seven selected loading displacements, 0.025 mm, 0.04 mm, 0.05 mm, 0.1 mm, 0.15 mm, 0.6 mm, and 1 mm, respectively. In Figure 9, σ_s and D, for the same loading displacement, are plotted in the same color. Solid lines represent σ_s, while dashed lines denote D. Figures 9(a)–9(c) are for the undamage stage, partial damage stage, and complete damage stage, respectively. The undamage stage corresponds to the stage when the loading displacement is less than 0.04 mm. Two loading displacements of 0.025 mm and 0.04 mm are selected in the undamaged stage. As seen from Figure 9(a), σ_s gradually decreases from the loading end to the other end of the track slab, with increasing peak values for larger loading displacements. D keeps zero for both of the two cases because no damage occurs. When the loading displacement is larger than 0.04 mm, the damage will occur firstly at the loading end and then gradually extends to the other end as the loading displacement increases. Figure 9(b) shows σ_s and D for three selected loading displacements of 0.05 mm, 0.1 mm, and 0.15 mm. In each σ_s curve, the whole track slab includes two zones: one is the damaged zone from the loading end to a certain point, where σ_s is very close to σ_s^0. The rest zone of the track slab is the zone without damage. In the damaged zone, a slight reduction of σ_s from σ_s^0 and the attenuation of D from the loading end can be observed. In the undamaged zone, D keeps zero and σ_s gradually decreases. The larger the loading displacement, the longer the length of the damaged zone, and hence the greater the maxima of D. The distribution of σ_s and δ_s on the entire track slab for the three loading displacements is plotted in Figure 10 which exhibits the development of the interfacial displacement from the loading end to the entire track slab. When the loading displacement reaches 0.15 mm, the damage extends to the whole interface. Afterward, σ_s shows an overall reduction, whereas D shows an overall increase for

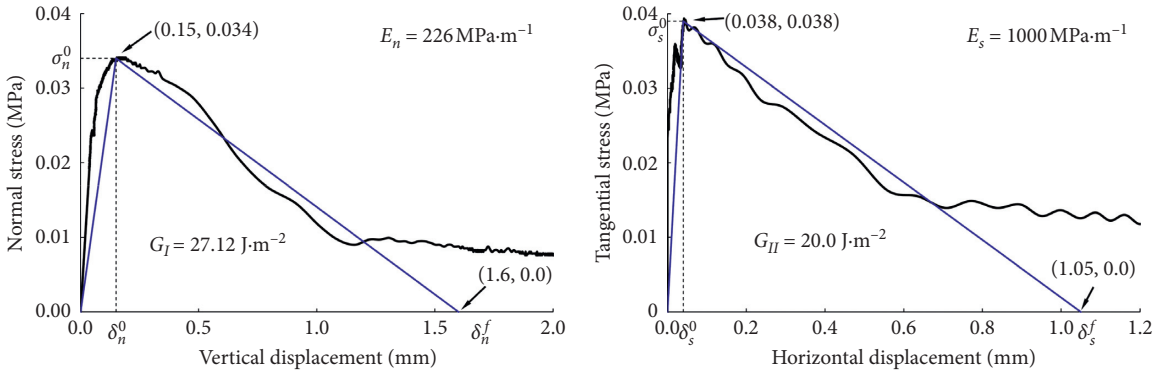

Figure 7: Force-displacement curve of the vertical (a) and horizontal push plate test (b).

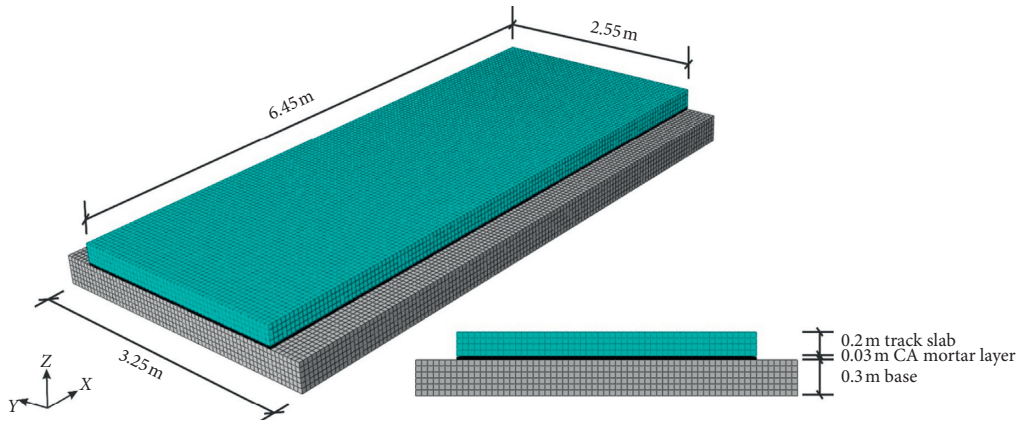

Figure 8: Finite element model of CRTS II SBTS.

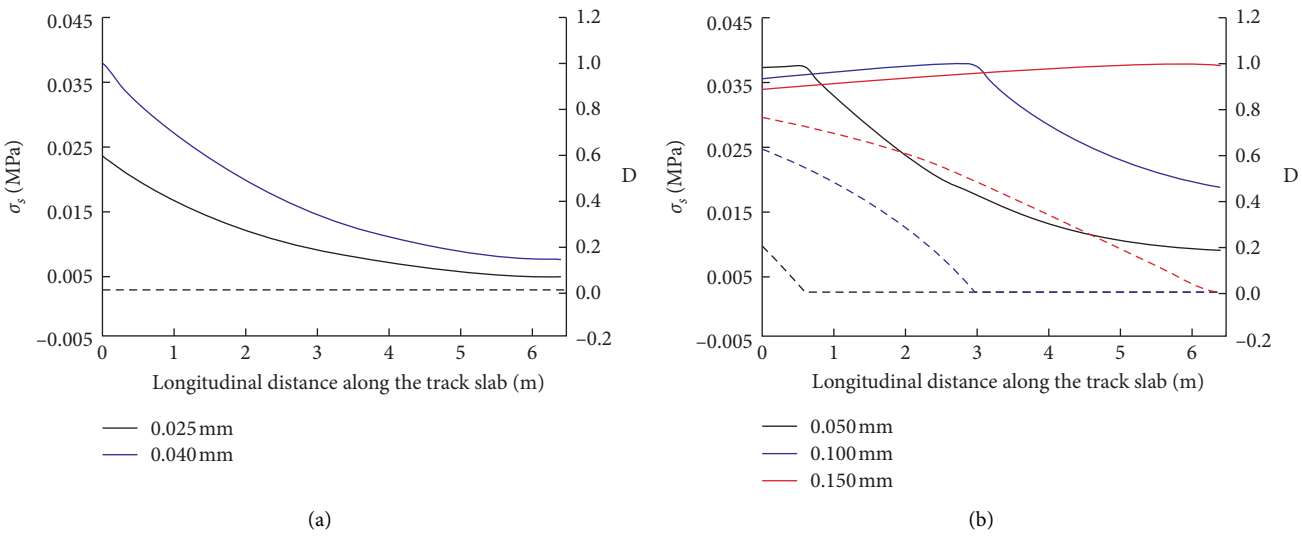

Figure 9: Continued.

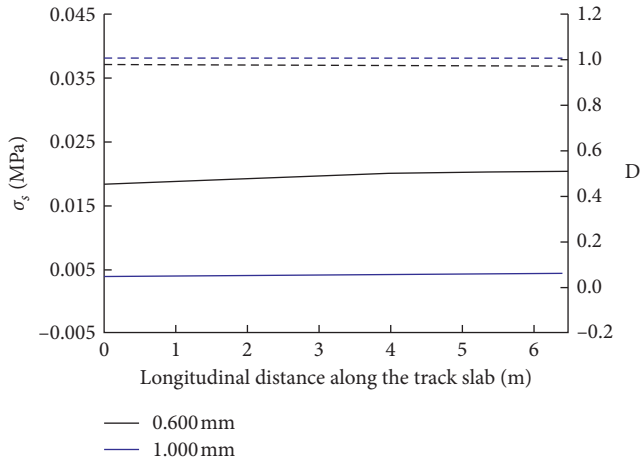

(c)

Figure 9: Distribution of σ_s and D on the track slab. (a) Undamage stage. (b) Partial damage stage. (c) Complete damage stage.

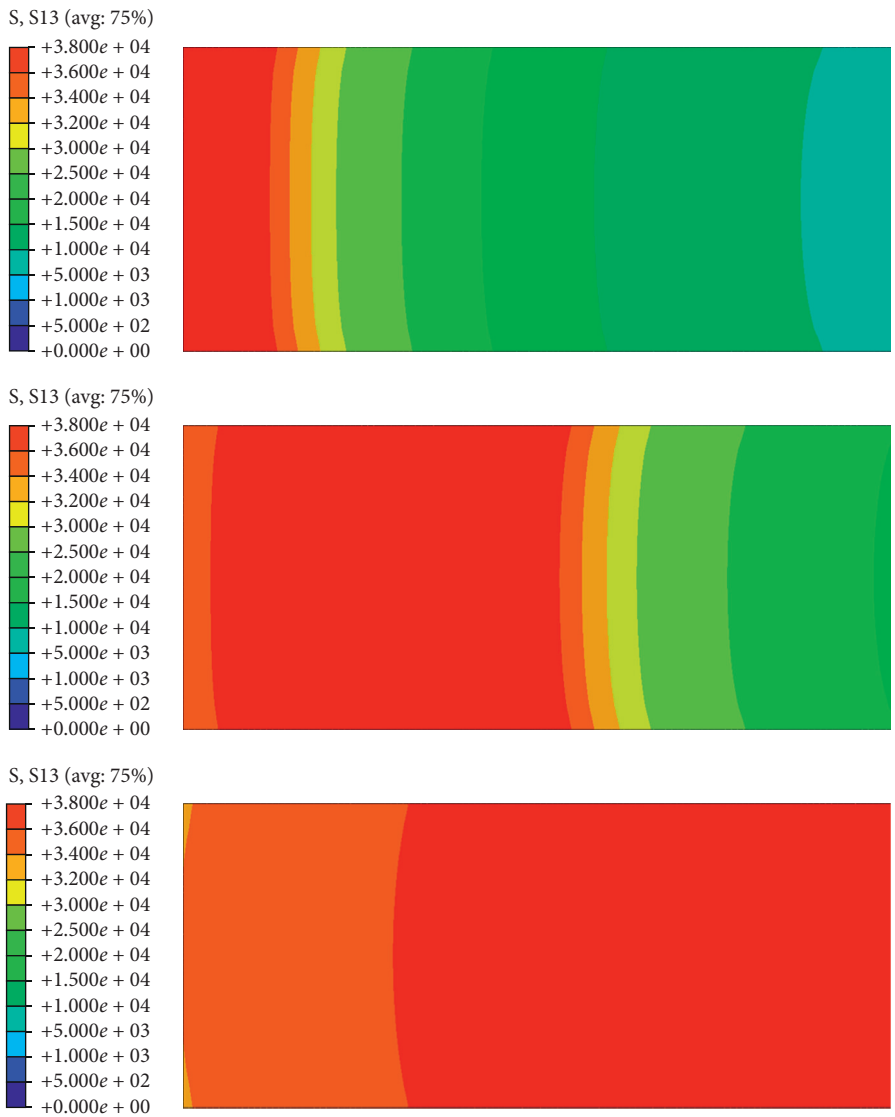

(a)

Figure 10: Continued.

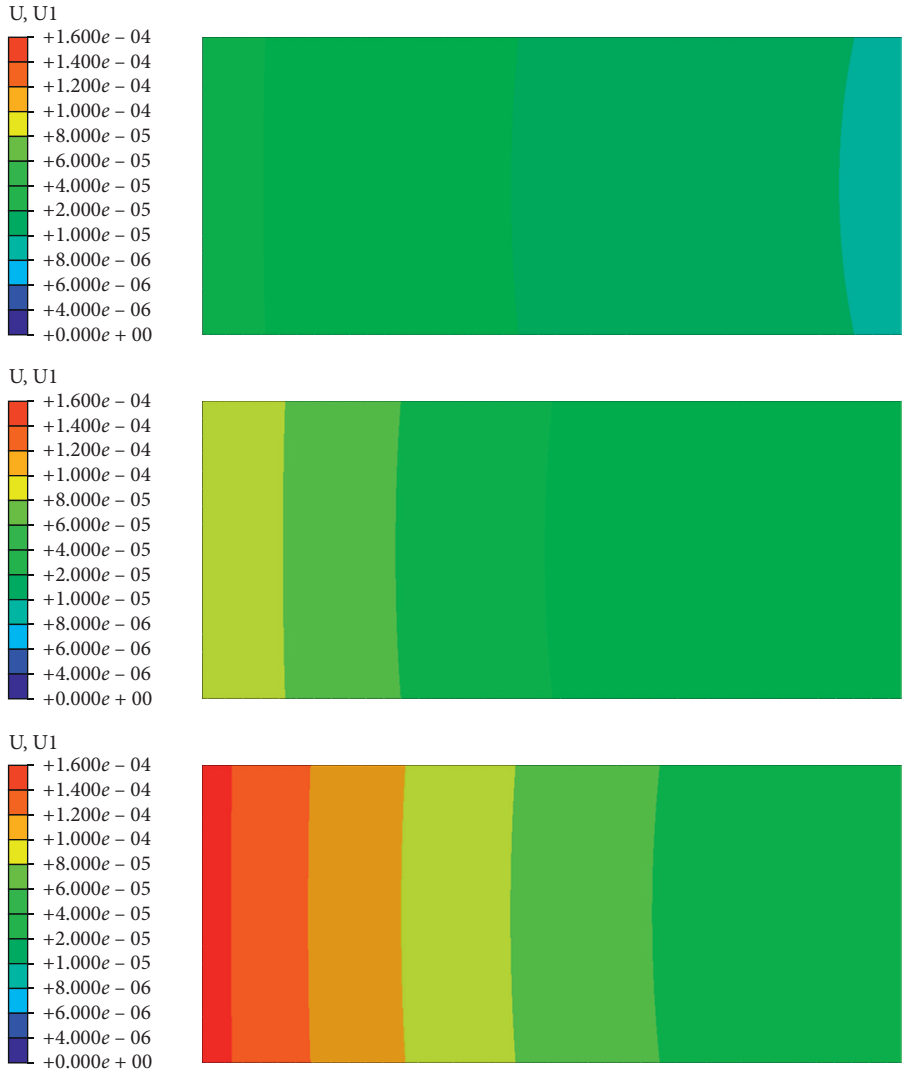

(b)

Figure 10: The interfacial tangential stress and displacement on the track slab. (a) Development of interfacial tangential stress. (b) Development of interfacial tangential displacement.

Table 1: Comparison of the theoretical and simulated L_0 for various E_s.

E_s (MPa · m^{-1})	Theoretical (m)	FEA (m)	Error (%)
30	37.42	38.00	1.6
100	20.49	18.50	9.7
1000	6.48	6.10	5.9
5000	2.90	2.90	0.0

Table 2: Comparison of the theoretical and simulated L_D for various G_{IIC}.

G_{IIC} (J · m^{-2})	λ	Theoretical (m)	FEA (m)	Error (%)
5	1.04	6.71	6.50	3.1
10	1.76	11.42	10.70	6.3
20	2.79	18.11	16.00	11.7
40	4.26	27.58	22.50	18.4

larger loading displacements (Figure 9(c)). When the loading displacement reaches 1 mm, σ_s is close to zero, and D is approximately 1, which indicates the occurrence of delamination.

To verify the reliability of the linear proportional distribution method, L_0 and L_D are simulated for various E_s and G_{IIC}. To represent the scenario long track slab, the finite element model in Figure 8 is enlarged to be 50 meter long. L_0 for E_s of 30, 100, 1000, and 5000 MPa/m is first simulated with fixed σ_s^0 of 0.038 MPa and G_{IIC} of 20 J/m^2. The simulated L_0 is compared with the theoretical L_0 calculated using equation (6), as listed in Table 1. From Table 1, L_0 from the FEA is very close to the theoretical L_0. L_0 decreases as E_s increases. For E_s of 30 MPa/m, L_0 is approximately six times the length of a single track slab and 5.6 times of L_0 for E_s of 1000 MPa/m. L_D for G_{IIC} of 5, 10, 20, and 40 J/m^2 are then simulated with fixed σ_s^0 of 0.038 MPa and E_s of 1000 MPa/m. The simulated L_D is listed in Table 2 together with the

theoretical L_D calculated based on λ of equation (15). From Table 2, L_D from the FEA is generally closed to the theoretical L_D. The difference between the theoretical and simulated L_D becomes larger as G_{IIC} increases. The agreement between the theoretical and simulated solutions in Tables 1 and 2 indicates that the linear proportional distribution method is effective to analyze the force-displacement variation for a single track slab.

5. Conclusions

In this paper, the push plate test of CRTS II SBTS is investigated by theoretical analysis, experiments, and numerical simulation. In the theoretical analysis, a series of analytical formulas of the force-displacement relationship is derived. In the numerical simulation, a bilinear CZM is adopted to simulate the interface within CRTS II SBTS. The parameters of the CZM are determined by scale push plate test. Particularly, a scale vertical push plate test instead of the traditional splitting tensile test is carried out to determine the normal cohesive parameters. The simulation exhibits the variation of the interfacial tangential stress σ_s and total stiffness damage D during the entire loading process. The results are as follows:

(1) The force-displacement curve constructed by the linear proportional distribution method agrees well with those obtained from full-scale test. This proves the reliability of the proposed method in analyzing the force-displacement variation of CRTS II SBTS in the horizontal push plate test.

(2) The simulation indicates that there is a partial damage stage between the undamage stage and the complete damage stage. This three-stage variation of the interfacial bond properties differs from the two-stage assumption of the bilinear CZM. However, the three-stage assumption is closer to the real force-displacement variation observed in the full-scale push plate test, and the linear proportional distribution method proposed in this paper is capable to reproduce this three-stage variation of the interfacial bond properties.

(3) The maximum affected length on the track slab in the damage stage, L_0, and the maximum damaged length in the undamage stage, L_D, are independent of the horizontal load. They only depend on the elastic modulus E, the interfacial stiffness E_s, the height of the track slab h, and the cohesive parameters δ_s^0 and δ_s^f. L_0 and L_D given by the FEA are very close to those defined by the proposed linear proportional distribution method. This proves the reliability of the proposed method and the capability of scale push plate test in determining the cohesive parameters.

However, this does not imply that the full-scale push plate test can be replaced fully by the scale push plate tests. The full-scale push plate test is of high cost and complicated, but it can minimize the effects from the construction quality, specimen size, loading condition, and other factors. A practical way to determine tangential cohesive parameters is to carry out a certain amount of scale test with the validation of several full-scale test. For the determination of the normal cohesive parameters, the scale vertical push plate test is the most practical way so far due to the challenge of setting up a full-scale vertical push plate test with uniform interfacial force during the entire loading process.

The size of the specimen in the scale test in this paper is estimated based on engineering experience with the aid of several times of trial test, which ensures that delamination will not occur too early during the test. The size effect is not involved considering that the scope of this paper is rather in building an integrated analysis approach using theoretical, experimental, and numerical tools than specifically discussing any of the three tools. In the future work, the effect of changing the specimen size on the test results would be investigated [18]. The parameters of the CZM are actually temperature dependent. However, for the bilinear CZM used in this paper, there is no existing research that reports the temperature variability of the key parameters (the interfacial stiffness, the interfacial strength, and the fracture toughness). In future works, push plate test under the load of time-varying temperature could be conducted by the use of a large scale temperature cabinet, from which the temperature variability of the parameters of the CZM could be investigated. The interface bond behavior is likely to degrade under the daily repeated living load of the train. This will increase the possibility of damage initiation and expansion. However, the fatigue of the interfacial bond behavior is out of the evaluation of push plate test and could be investigated in the future with the aid of fatigue test of CRTS II SBTS [19, 20].

Data Availability

The data used to support the findings of this study are available from the corresponding author upon request.

Conflicts of Interest

The authors declare no conflicts of interest with respect to the research, authorship, and/or publications of this article.

Acknowledgments

The research was financially supported by the National Natural Science Foundation of China (Grants nos. 51708459 and 51878578) the Project of Science and Technology Research and Development of China Railway Co., Ltd. (Grant no. K2020G007), and the Open Foundation of Undergraduate-Oriented Engineering Practice Project of Key Laboratory of Southwest Jiaotong University (ZD2020010035).

References

[1] Y. Li, J. Chen, J. Wang, X. Shi, and L. Chen, "Study on the interface damage of CRTS II slab track under temperature load," *Structure*, vol. 26, pp. 224–236, 2020.

[2] G. Dai, H. T. Su, W. S. Liu, and B. Yan, "Temperature distribution of longitudinally connected ballastless track on

bridge in summer," *Journal of Central South University*, vol. 48, no. 4, pp. 1073–1080, 2017.

[3] G. Zhao, L. Gao, L. Zhao, and Y. L. Zhong, "Analysis of dynamic effect of gap under CRTS II track slab and operation evaluation," *Journal of the China Railway Society*, vol. 39, no. 1, pp. 1–10, 2017.

[4] G. Zhao and Y. Liu, "Mechanism analysis of delamination of CRTS II slab ballastless track structure," *Journal of the China Railway Society*, vol. 42, no. 7, pp. 117–126, 2020.

[5] J. Liu, X. Wen, Z. Zhang, S. Li, and Z. Zeng, "Influence of the stabilizer on interfacial bonding behavior of cement asphalt mortar in slab ballastless track," *Journal of Materials in Civil Engineering*, vol. 30, no. 10, Article ID 04018245, 2018.

[6] J. Ren, J. Wang, X. Li, K. Wei, H. Li, and S. Deng, "Influence of cement asphalt mortar debonding on the damage distribution and mechanical responses of CRTS I prefabricated slab," *Construction and Building Materials*, vol. 230, Article ID 116995, 2020.

[7] Y. Zhong, L. Gao, P. Wang, and S. Liang, ""Mechanism of interfacial shear failure between CRTS II slab and CA mortar under temperature loading," *Engineering Mechanics*, vol. 5, no. 2, pp. 230–237, 2018.

[8] J. Zhang, S. Zhu, C. Cai, M. Wang, and H. Li, "Experimental and numerical analysis on concrete interface damage of ballastless track using different cohesive models," *Construction and Building Materials*, vol. 263, Article ID 120859, 2020.

[9] Y. Zhang, K. Wu, L. Gao, X. Cai, and S. Yan, "Comparison of viscoelastic and elastic analysis of slab track under temperature gradient loading," *Journal of Central South University*, vol. 51, no. 7, pp. 2028–2038, 2020.

[10] G. Dai and M. Su, "Full-scale field experimental investigation on the interfacial shear capacity of continuous slab track structure," *Archives of Civil and Mechanical Engineering*, vol. 16, no. 3, pp. 485–493, 2016.

[11] X. Chen, Y. Zhu, D. Cai, G. Xu, and T. Dong, "Investigation on interface damage between cement concrete base plate and asphalt concrete waterproofing layer under temperature load in ballastless track," *Applied Sciences*, vol. 10, no. 8, p. 2654, 2020.

[12] D. Li, *Performance of CRTS II slab ballastless track on the high speed railway bridge*, Ph.D. thesis, China Academy of Railway Science, Beijing, China, 2016.

[13] X. Liu, C. Su, D. Liu, F. Xiang, C. Gong, and P. R. Zhao, "Research on the bond properties between slab and CA mortar and the parameters study of cohesive model," *Journal of Railway Engineering Society*, vol. 34, no. 3, pp. 22–28, 2017.

[14] Q. Shen, W. Chen, C. Liu, W. Zou, and L. Pan, "The tensile strength and damage characteristic of two types of concrete and their interface," *Materials*, vol. 13, no. 1, pp. 16–34, 2019.

[15] S. Zhu, M. Wang, W. Zhai et al., "Mechanical property and damage evolution of concrete interface of ballastless track in high-speed railway: experiment and simulation," *Construction and Building Materials*, vol. 187, pp. 460–473, 2018.

[16] Y. Xu, D. Yan, W. Zhu, and Y. Zhou, "Study on the mechanical performance and interface damage of CRTS II slab track with debonding repairment," *Construction and Building Materials*, vol. 257, Article ID 119600, 2020.

[17] D. Ranz, J. Cuartero, L. Castejon, R. Miralbles, and H. Malon, "A cohesive zone model approach in interlaminar behavior of carbon/epoxy laminated curved beams," *Composite Structures*, vol. 238, Article ID 111983, 2020.

[18] J. Liu, W. Yu, and X. D, "Size effect on static splitting tensile strength of concrete experimental and numerical studies," *Journal of Materials in Civil Engineering*, vol. 32, no. 10, Article ID 04020308, 2020.

[19] Z. Zeng, J. Wang, S. Shen, P. Li, A. Shuaibu, and W. Wang, "Experimental study on evolution of mechanical properties of CRTS III ballastless slab track under fatigue load," *Construction and Building Materials*, vol. 210, pp. 639–649, 2019.

[20] L. Zhou, L. Yang, Z. Shan, X. Peng, and A. Mahunon, "Investigation of the fatigue behaviour of a ballastless slab track-bridge structural system under train load," *Applied Sciences*, vol. 9, no. 17, Article ID 3625, 2019.